Nuclear Materials and Energy 12 (2017) 247–252

Contents lists available at ScienceDirect

Nuclear Materials and Energy

journal homepage: www.elsevier.com/locate/nme

High-Z material erosion and its control in DIII-D carbon divertor

R. Ding[a,b,*], D.L. Rudakov[c], P.C. Stangeby[d], W.R. Wampler[e], T. Abrams[a], S. Brezinsek[f], A. Briesemeister[g], I. Bykov[c], V.S. Chan[h], C.P. Chrobak[h], J.D. Elder[d], H.Y. Guo[h], J. Guterl[a], A. Kirschner[f], C.J. Lasnier[i], A.W. Leonard[h], M.A. Makowski[i], A.G. McLean[i], P.B. Snyder[h], D.M. Thomas[h], D. Tskhakaya[j,k], E.A. Unterberg[g], H.Q. Wang[a], J.G. Watkins[e]

[a] Oak Ridge Associated Universities, Oak Ridge, TN, USA
[b] Institute of Plasma Physics, Chinese Academy of Sciences, PO Box 1126, Hefei, Anhui 230031, PR China
[c] University of California San Diego, 9500 Gilman Drive, La Jolla, CA 92093-0417, USA
[d] University of Toronto, Institute for Aerospace Studies, Toronto, M3H 5T6, Canada
[e] Sandia National Laboratory, P.O. Box 5800, Albuquerque, NM 87185, USA
[f] Forschungszentrum Jülich GmbH, Institute of Energy and Climate Research-Plasma Physics, Jülich 52425, Germany
[g] Oak Ridge National Lab, Oak Ridge, TN, USA
[h] General Atomics, PO Box 85608, San Diego, CA 92186-5608, USA
[i] Lawrence Livermore National Laboratory, 7000 East Avenue, Livermore, CA 94550, USA
[j] Fusion@ÖAW, Institute of Applied Physics, TU Wien, Wiedner Hauptstraße 8-10, Vienna 1040, Austria
[k] Institute for Theoretical Physics, University of Innsbruck, Innsbruck A-6020, Austria

ARTICLE INFO

Article history:
Received 22 July 2016
Revised 7 December 2016
Accepted 9 March 2017
Available online 16 March 2017

ABSTRACT

As High-Z materials will likely be used as plasma-facing components (PFCs) in future fusion devices, the erosion of high-Z materials is a key issue for high-power, long pulse operation. High-Z material erosion and redeposition have been studied using tungsten and molybdenum coated samples exposed in well-diagnosed DIII-D divertor plasma discharges. By coupling dedicated experiments and modelling using the 3D Monte Carlo code ERO, the roles of sheath potential and background carbon impurities in determining high-Z material erosion are identified. Different methods suggested by modelling have been investigated to control high-Z material erosion in DIII-D experiments. The erosion of Mo and W is found to be strongly suppressed by local injection of methane and deuterium gases. The ^{13}C deposition resulting from local $^{13}CH_4$ injection also provides information on radial transport due to $\mathbf{E} \times \mathbf{B}$ drifts and cross field diffusion. Finally, D_2 gas puffing is found to cause local plasma perturbation, suppressing W erosion because of the lower effective sputtering yield of W at lower plasma temperature and for higher carbon concentration in the mixed surface layer.

© 2017 The Authors. Published by Elsevier Ltd.
This is an open access article under the CC BY-NC-ND license.
(http://creativecommons.org/licenses/by-nc-nd/4.0/)

1. Introduction

High-Z materials such as tungsten (W) will be used for plasma facing materials in the ITER divertor [1] and are expected to be used in future fusion devices. The main disadvantage of high-Z materials is that the generation of high-Z impurities and their penetration into the core plasma can cause large radiation losses, resulting in poor plasma performance. It is essential to understand and control high-Z impurity sources which will help to reduce high-Z impurity concentration in the core plasma. The most common high-Z impurity source in tokamaks is physical sputtering by impinging ions. Since the threshold energy for sputtering by the fuel ions is high, the sputtering rates for high-Z materials are mainly determined by other impurities, low-Z ions especially when mixed materials are used for plasma facing components [2, 3]. It was also found that significant amounts of eroded high-Z materials can be locally redeposited resulting in much lower net erosion rates compared to gross erosion rates [4, 5]. Simulation of dedicated experiments under well-controlled and characterized conditions can aid understanding of the underlying physics of erosion and redeposition of high-Z materials.

Since the DIII-D tokamak has full graphite PFCs, high-Z material erosion in a mixed materials environment can be readily studied, which can have implications for ITER with its low-Z beryllium first

* Corresponding author at : Division of Tokamak Physics, 350 Shushanhu Road, PO Box 1126, Hefei, Anhui 230031, PR China.
E-mail address: rding@ipp.ac.cn (R. Ding).

http://dx.doi.org/10.1016/j.nme.2017.03.012
2352-1791/© 2017 The Authors. Published by Elsevier Ltd. This is an open access article under the CC BY-NC-ND license. (http://creativecommons.org/licenses/by-nc-nd/4.0/)

wall and high-Z tungsten divertor. The divertor materials evaluation system (DiMES) in the lower divertor of DIII-D is an excellent platform for carrying out well-controlled experiments on plasma material interactions [6]. It enables measurements of gross and net erosion rates of high-Z materials by ion beam analysis of material samples before and after plasma exposure [7, 8]. Edge diagnostics such as floor Langmuir probes and divertor Thomson scattering provides the local plasma conditions for the numerical simulations. Within this work, the three-dimensional Monte Carlo code ERO [9], which simulates material erosion, migration and redeposition, is used to model dedicated DiMES experiments on DIII-D. The critical parameters determining high-Z material erosion such as the magnetic pre-sheath properties and background impurities have been identified by comparison of measured and modelling results. Several different methods have been studied to suppress high-Z material erosion in the DIII-D divertor.

2. DIII-D experiments and ERO-OEDGE modelling

To provide a good benchmark for the code, the conditions for the DIII-D experiments described here are kept as simple as possible. All the experiments were carried out in L-mode deuterium discharges with a lower single null magnetic configuration. Thin molybdenum (Mo) or W coating samples was exposed to well-diagnosed plasma conditions using DiMES. Each sample was exposed to several reproducible plasma discharges. During the plasma current flattop, the outer strike point was kept near the sample to guarantee a local net erosion condition. The thickness of the sample coating was measured by Rutherford backscattering (RBS) before and after exposure to determine the time-averaged erosion rates, which are compared with modelling. The ERO code has been applied to DiMES experiments to address high-Z material erosion issues [10]. It calculates physical sputtering and chemical erosion and traces the eroded particles in a fixed background plasma. The main input required for ERO modelling is the plasma background which is reconstructed by the interpretive OEDGE code using the Onion Skin Model [11]. The OEDGE code solves the 1D fluid conservation equations along the magnetic field with the input boundary condition of plasma parameters on divertor targets measured by Langmuir probes. The 2D distribution of plasma density, temperature, flow velocity and parallel electric field from OEDGE calculations are used for ERO simulation volume, in which toroidal symmetry is assumed. The radial profiles of electron density (n_e) and temperature (T_e) across DiMES at the divertor target for Mo exposure and methane injection experiments are shown in Fig. 1 as measured by Langmuir probes. The modelling aids in understanding of the experiments and also suggests new techniques to control erosion of high-Z materials.

2.1. Sheath effects

A non-spectroscopic method which uses a small spot of high-Z material coating with a diameter of 1 mm has been developed to measure gross erosion rates in DIII-D [8, 12]. It is assumed that under typical L-mode conditions the redeposition of eroded material on the 1 mm spot is negligible, because the ionization mean free path of eroded neutrals is comparable to the sample size. This assumption is confirmed by modelling with both REDEP/WBC [13] and the ERO code. The redeposition ratio for a 1 mm sample is only 3–4% according to ERO modelling. With a simultaneously exposed 1 cm diameter sample, the net/gross erosion ratio or redeposition ratio can be obtained. From measurements for a 1 cm sample, the redeposition ratio of Mo is 44% while W has a higher redeposition ratio of 63% [12]. Modeling with the ERO code indicates that the high local re-deposition ratio is mainly controlled

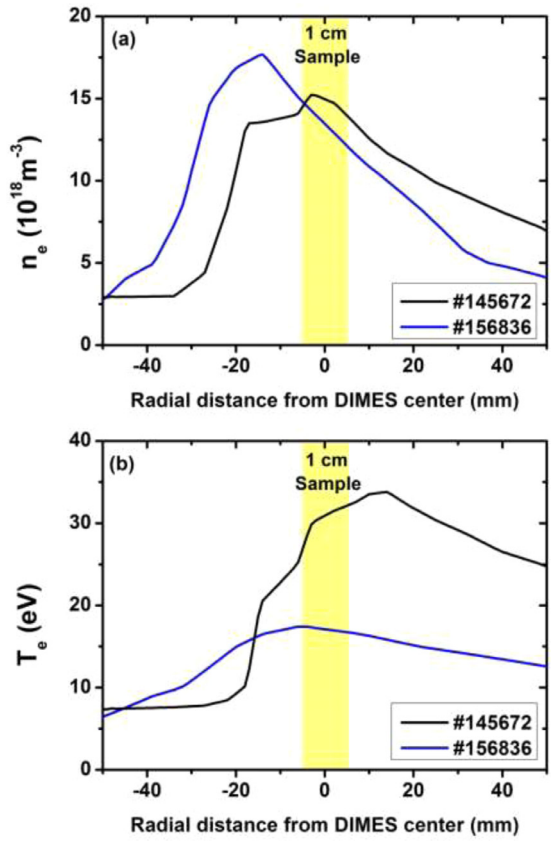

Fig. 1. Radial profiles of (a) electron density and (b) electron temperature at divertor target for Mo exposure (#145672) and methane injection (#156836) experiments measured by Langmuir probes.

by the electric field and plasma density within the magnetic pre-sheath [10]. During the experiment described here, the magnetic field lines intersect the material surface at a very shallow angle of 1.5° The magnetic pre-sheath potential drop is increased with decreasing the angle between the magnetic field lines and the material surface [14]. The standard sheath model used in the ERO code is the Brooks' model using a fitting parameter to define the fraction of the magnetic pre-sheath [15]. Recent fluid analysis by Stangeby concludes that the Debye sheath disappears when the angle is small enough, if the total potential drop across both the magnetic pre-sheath and the Debye sheath is assumed not to change [16]. Kinetic simulations using the particle-in-cell (PIC) code BIT1 with one spatial and three velocity dimensions is used to model the sheath properties for comparison with the fluid model [17]. All three models have been tested in the ERO code to calculate the Mo redeposition ratio, as shown in Fig. 2. Similar Mo re-deposition ratios were obtained from ERO modeling using the three models, all being close to the measured value of 44% for a 1 cm sample. The average Mo redeposition ratio increases with increasing diameter of the sample. Most of the sputtered Mo atoms are ionized within the magnetic pre-sheath region and therefore the strong electric field towards the material surface plays an important role in Mo redeposition.

Since the redeposition ratio is mainly determined by the magnetic pre-sheath, ERO simulations have also been performed for a reduced sheath potential. The potential profile for a non-floating material surface can be calculated from fluid analysis [16]. As seen in Fig. 3, when the 1 cm Mo sample surface is biased with positive voltage relative to the floating potential, the Mo redeposition ratio is not reduced, but shows an even slight increase. Although the re-

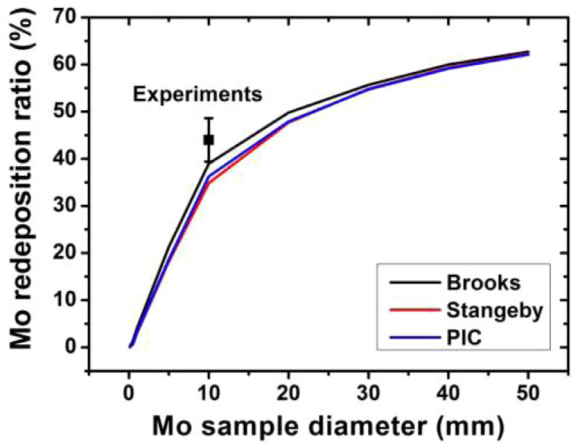

Fig. 2. The dependence of the Mo redeposition ratio on sample diameter using three different sheath models in ERO compared with experiment.

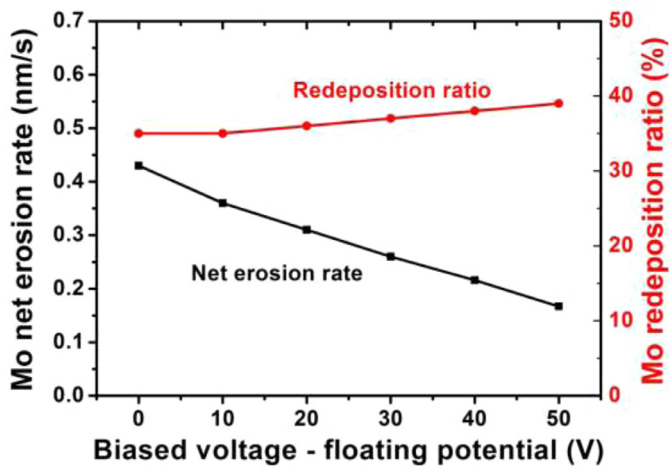

Fig. 3. ERO modelled net erosion rate and redeposition ratio of the 1 cm Mo sample as a function of biased voltage relative to the floating potential.

duced total potential drop leads to lower sheath electric field, the electron density within the magnetic pre-sheath becomes larger according to the Boltzmann relation. Higher electron density leads to a shorter ionization mean free path and thus higher redeposition. That is, the sheath electric field and electron density within the magnetic pre-sheath have opposite effects on the redeposition ratio. Decreasing sheath potential drop also results in lower gross erosion rate because the sputtering yield is reduced due to the lower ion incident energy on the surface. In the ERO modeling, it is assumed that the ion incident flux does not change within the biased voltage range Therefore the Mo net erosion rate can be suppressed by positive biasing since the Mo redeposition ratio is not decreased. As shown in Fig. 3, the Mo net erosion rate is reduced almost linearly by more than a factor of 2 when the biased voltage is 50 V higher than the floating potential. New experiments have been recently carried out in DIII-D to test this ERO prediction, in which the Mo sample was biased to different voltages. A strong correlation of Mo erosion with biasing voltage has been obtained in the experiments. The detailed results of these experiments will be reported elsewhere.

2.2. Local $^{13}CH_4$ gas injection

Erosion of high-Z materials by background fuel ions is usually very low due to the high sputtering thresholds, and low-Z impurity sputtering dominates erosion, especially for W. Since DIII-D has full graphite wall coverage, carbon impurities play an important role in material erosion and deposition. ERO modelling indicates that higher carbon impurity concentrations in the plasma can reduce the net erosion rate of Mo, because the effective sputtering rate of Mo is reduced due to higher carbon deposition in the mixed material surface layer [10]. In ERO simulations, the carbon ratio in the surface interaction layer is determined by the overall erosion and deposition flux balance of different species on the material surface. If the carbon concentration in the plasma is high enough, the metal surface will be in a net deposition condition. Therefore, high-Z material erosion can be controlled by the low-Z impurity content of the plasma.

The background carbon level can be increased by local methane injection close to the metal sample. In DIII-D, a capillary opening through a hole in a floor tile at the same major radius at the DiMES centre is used for the local gas puffing [18]. The hole is 12 cm upstream of the DiMES centre in the toroidal direction. To distinguish the injected carbon from the background ^{12}C in post-mortem analysis, $^{13}CH_4$ is injected from the capillary. In the experiment described here, a 1 cm Mo sample coating was located 1 cm upstream from the DiMES centre in order to accommodate an embedded Langmuir probe (see Fig. 4(d) in [18]). $^{13}CH_4$ was injected at a rate of 1.8 Torr-l/s during three L-mode repeat discharges (shots #156836 - #156838). The emission from the gas injection was observed from the top using a CCD camera with a 430.5 nm CD/CH molecular band filter. The spectroscopic signal of MoI emission became negligible during methane puffing. After the experiment, carbon deposition could be clearly seen as a toroidal stripe on the DiMES head. The Mo sample experienced a net-deposition condition and Mo erosion was below the detection limit for RBS measurements. Both ^{13}C and ^{12}C deposition on the Mo sample were measured by nuclear reaction analysis (NRA) with 2.5 MeV ^{3}He. The ^{13}C areal density was found to be higher than the ^{12}C areal density by nearly an order of magnitude, which indicates that the carbon deposition was mainly due to the external gas injection.

^{13}C deposition from $^{13}CH_4$ injection was modelled by the ERO code. Methane molecules are launched in the code at the injection aperture with a cosine angular distribution and Maxwell energy distribution. The methane molecules are dissociated and ionized into various hydrocarbon species due to the interaction with plasma electrons and ions. These processes are calculated using the corresponding reaction rate coefficients [19, 20]. In the modelling, the effective sticking coefficient for hydrocarbon molecules hitting material surfaces is assumed to be 0 according to the previous studies [21]. The light emission from different species can be simulated by the ERO code depending on the density distribution and effective photon emission rate coefficients of the corresponding species. Fig 4 shows the ERO modelled 2D pattern of CH and CIII light emission resulting from $^{13}CH_4$ injection. Due to fast break-up of molecular species, CH band light is more localized near the injection point. The broader emission pattern of CIII indicates that the carbon ions can penetrate deeper into the plasma and move in downstream direction due to frictional entrainment with the main ion flow. The ^{13}C deposited on the DiMES head as a toroidal stripe observed in the experiment is due to the longer transport of carbon ions.

The measured ^{13}C deposition profile on the Mo sample provides a good benchmark for ERO modelling on carbon transport. It is found that the ERO modelled radial coverage of ^{13}C strongly depends on $\mathbf{E} \times \mathbf{B}$ drifts and the cross field diffusion coefficient. As seen in Fig. 5, if both the sheath electric field E and the diffusion coefficient D are assumed to be 0, the radial ^{13}C deposition profile is rather symmetric relative to the radial location of gas injection. When E is taken into account, the modelled deposition profile is shifted in the $\mathbf{E} \times \mathbf{B}$ direction. The measured ^{13}C deposition from experiment is also higher in the radial inboard direction,

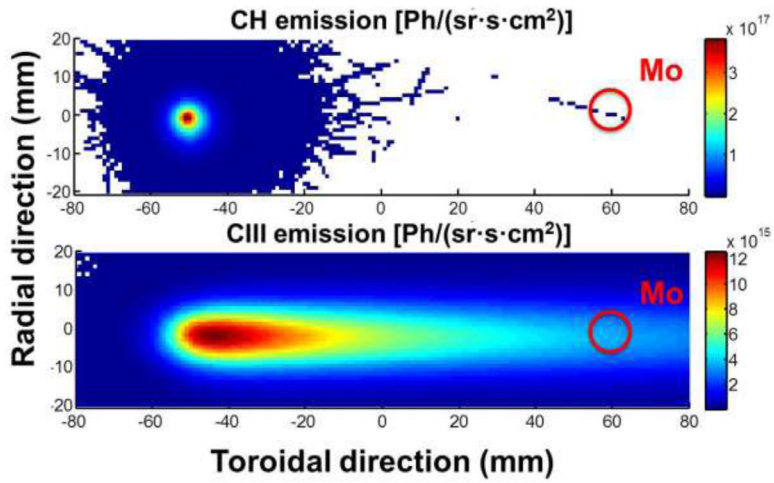

Fig. 4. Modelled 2D emission (top view) of CH (upper) and CIII (lower) resulting from local $^{13}CH_4$ injection.

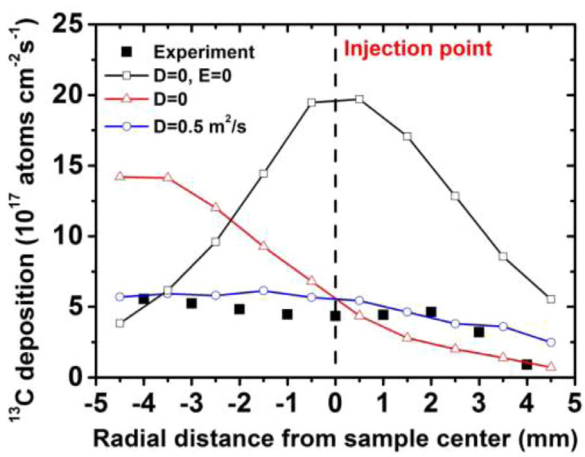

Fig. 5. Comparison of experimental and ERO modelled radial profiles of ^{13}C deposition rates on a Mo sample for different assumptions on the cross field diffusion coefficient and sheath electric field.

which is mainly due to $\mathbf{E} \times \mathbf{B}$ drift. A higher diffusion coefficient D leads to lower ^{13}C deposition on the Mo sample and the profile becomes broader. For $D = 0.5\,m^2\,s^{-1}$, the modelled ^{13}C deposition profile shows good agreement with the experiments.

2.3. Local D_2 gas injection

Deuterium gas injection was also performed to test the mitigation of high-Z material erosion by local plasma perturbation. Two pre-characterized samples with both 1 cm and 1 mm W coatings that are indicative of the net and gross erosion rates were exposed with and without D_2 gas puffing. D_2 gas was injected at the same location as in previous methane injection experiments. Before the W sample was exposed, a built-in Langmuir probe was installed on the DiMES head and exposed to several discharges with D_2 gas injection in order to measure the local plasma parameters before and during the gas injection. As shown in Fig. 6, during the discharge, the D_2 injection started at around 2.5 s with an increasing rate to about 9 torr-l/s. Then at 4 s the injection rate was increased to about 15 torr-l/s. The embedded Langmuir probes data showed strong local perturbation of electron density and temperature due to the gas puffing. When the gas puff started, T_e was reduced from ~26 eV to below 10 eV and n_e increased by about a factor of 3. At the highest injection rate, plasma parameters changed slightly

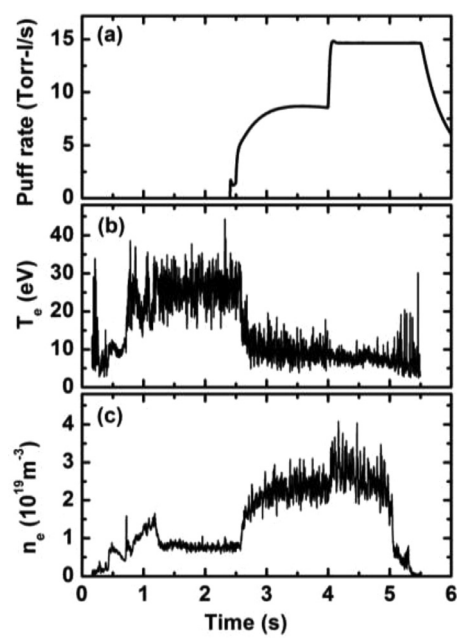

Fig. 6. Time traces of (a) D_2 puffing rate, (b) electron temperature and (c) electron density measured by the Langmuir probe embedded in DiMES head in shot #162765.

compared to the lower injection rate. There is no measurable effect on the global discharge parameters at the lower injection rate, but a global disturbance was observed after 4 s during the higher gas injection rate. Then the first W-coated sample was installed on the DiMES head instead of the Langmuir probe for three repeat discharges with the same time evolution of D_2 gas injection. The second W-coated sample was exposed for three repeat discharges to obtain the baseline erosion rate without gas injection. After exposure, the net erosion of 1 mm and 1 cm W spots on both samples were analysed by RBS. For the 1 mm spot, the W erosion without gas puffing is about $1.96\,(\pm 0.3) \times 10^{16}$ atoms cm^{-2} or 3.1 nm. With D_2 injection, the W erosion is reduced to about $1.2\,(\pm 0.3) \times 10^{16}$ atoms cm^{-2} or 1.9 nm. The net erosion profiles along toroidal and radial direction on the 1 cm W coating sample for the cases of both no gas puff and with gas puff are compared in Fig. 7. The average W net erosion for the 1 cm sample in the two cases are $1.54\,(\pm 0.3) \times 10^{16}$ atoms cm^{-2} and $0.78\,(\pm 0.3) \times 10^{16}$ atoms cm^{-2} respectively. The W erosion is significantly suppressed by D_2 gas in-

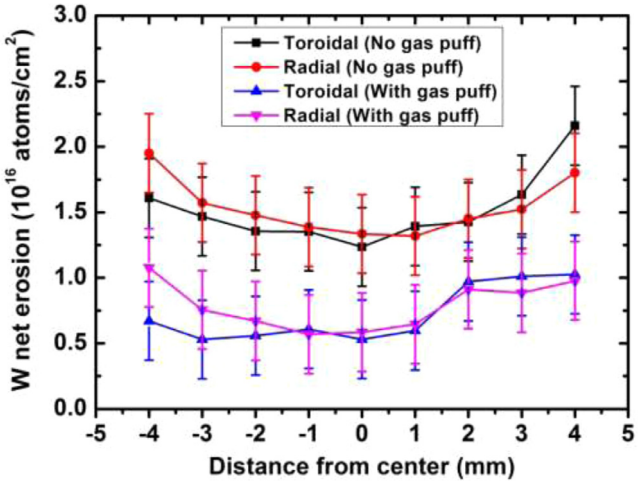

Fig. 7. RBS measurements of W net erosion profiles for 1 cm W sample with and without D_2 gas puff.

jection. The W erosion profiles in radial and toroidal directions are similar for both cases. Higher erosion near the edge of the 1 cm sample compared to the centre is due to the higher local redeposition at the centre. The net erosion ratio of 1 cm W to 1 mm W is decreased from 0.79 to 0.65 by gas puffing, indicating that the W redeposition ratio is increased due to gas puffing. The W net erosion rates are summarized and compared with modelling in Table 1.

ERO simulations have been performed for three cases using the averaged electron density and temperature measured by the embedded Langmuir probe: no gas puff ($n_e = 7.7 \times 10^{12}$ cm^{-3}, $T_e = 26$ eV), low D_2 injection rate ($n_e = 2.3 \times 10^{13}$ cm^{-3}, $T_e = 9.3$ eV) and high D_2 injection rate ($n_e = 2.6 \times 10^{13}$ cm^{-3}, $T_e = 7.7$ eV). The carbon concentration in the background plasma is assumed to be 1.8% according to the previous studies [10]. As seen from Table 1, for the non-puffing case, ERO gave a net erosion rate for the 1 mm W sample of 0.23 nm/s, which agrees well with the measured value of 0.26 nm/s. However, the modelled average net erosion rate for the 1 cm W sample is 0.11 nm/s, nearly a factor of 2 lower than the measured one of 0.2 nm/s. According to the measured erosion rates for the two sized samples, the net/gross erosion ratio is about 0.77. Therefore, the measured W redeposition ratio is only about 23%, much lower than the previous experiments of 63%, while the ERO modelled redeposition ratio is 53%, closer to the previous value. The large error bars shown in Fig. 7 also indicate large uncertainties of the measured erosion rate for the 1 cm sample. With D_2 gas puffing, the modelled W net erosion rates of both the 1 cm and 1 mm samples are reduced significantly. The gas injection reduces the local plasma temperature but increases the ion flux. The embedded Langmuir probe data shows that the ion saturation current during D_2 gas puffing is nearly double that without gas injection. The lower plasma temperature results in a much lower W sputtering yield. Furthermore, both lower plasma temperature and higher ion flux lead to more carbon deposition in the mixed material surface layer, which can reduce the effective sputtering yield of W through dilution. Therefore, the suppression of W erosion by D_2 gas puffing is mainly due to plasma cooling and higher carbon deposition on the W surface. As shown in Fig. 6, there are three stages of gas injection in one discharge, non-puffing, low injection rate and high injection rate. For a flattop time from 1 s to 5 s, the time proportions for the three stages are 37.5%, 37.5% and 25%, respectively. Therefore, the time-averaged modelled W net erosion rates are used for comparison with the experimental measurements, according to the time proportions of the three differ-

Table 1
Experimental and modelling results of W erosion and redeposition for 1 cm and 1 mm samples.

	Measured net erosion rate (nm/s)		ERO simulations					
			No gas puff $n_e = 7.7 \times 10^{12}$ cm^{-3} $T_e = 26$ eV		With D_2 gas puff $n_e = 2.3 \times 10^{13}$ cm^{-3} $T_e = 9.3$ eV		With D_2 gas puff $n_e = 2.6 \times 10^{13}$ cm^{-3} $T_e = 7.7$ eV		With D_2 gas puff (average)
	No gas puff	With gas puff	Net erosion rate (nm/s)	Redposition ratio	Net erosion rate (nm/s)	Redposition ratio	Net erosion rate (nm/s)	Redposition ratio	Net erosion rate (nm/s)
1 cm sample	0.2	0.1	0.11	53%	0.024	58%	0.015	57%	0.054
1 mm sample	0.26	0.16	0.23	6.8%	0.058	8.6%	0.035	8.1%	0.12

ent puffing conditions. The modelled average W net erosion rates with gas puff are 0.054 nm/s for the 1 cm sample and 0.12 nm/s for the 1 mm sample. As for the non-puffing case, the modelled net erosion rate for the 1 mm sample is in good agreement with the experiments, while the modelled erosion rate is about a factor of 2 lower than the measurements for the 1 cm sample. Although the measured W redeposition ratio is increased to 45% with gas injection, it is still lower than the modelled values. The modelled W redeposition ratio is also slightly increased in the gas puff case, which is mainly due to the shorter ionization mean free path of W atoms. The average W ionization distance perpendicular to the surface are 1.15 mm for the non-puffing case, 0.76 mm for the low injection rate and 0.79 mm for the high injection rate. Although the ionization rates are lower for lower electron temperature, much higher local electron density increases the ionization probability significantly.

3. Summary

Thin film W and Mo spot samples with different diameters were exposed to divertor plasma using DiMES in DIII-D to study high-Z material erosion and redeposition. The ERO-OEDGE code has been used to interpret the experimental observations and suggests new methods to control high-Z material erosion. A high local re-deposition ratio for eroded high-Z materials was observed in the experiments, which is mainly due to the electric field and plasma density within the magnetic presheath according to the modelling. Modelling also indicates that the net erosion rate can be reduced by reducing the sheath potential drop by positive biasing. Increasing carbon impurity levels in the background plasma can also suppress high-Z material erosion, which has been shown by DiMES experiments with local methane injection. $^{13}CH_4$ injection provides a good benchmark for the modeling and the ^{13}C deposition on the Mo surface is strongly influenced by $\mathbf{E} \times \mathbf{B}$ drifts and the cross field diffusion. Local D_2 gas injection upstream of the W sample not only reduced W net erosion rate but also increased the W redeposition ratio, mainly due to local plasma perturbation. The W effective sputtering yield is reduced due to both lower plasma temperature and higher carbon concentration in the surface interaction layer. The larger W redeposition rate is mainly controlled by shorter W ionization length resulting from the significantly increased plasma density.

Acknowledgements

This material is based upon work supported by the US Department of Energy, Office of Science, Office of Fusion Energy Sciences and Office of Advanced Scientific Computing Research through the Scientific Discovery through Advanced Computing (SciDAC) project on Plasma-Surface Interactions, under Award No. GA-DE-SC0008698, using the DIII-D National Fusion Facility, a DOE Office of Science user facility, under Awards DE-AC05-06OR23100, DE-FG02-07ER54917, DE-AC05-00OR22725, DE-FC02-04ER54698, and DE-AC52-07NA27344. Sandia National Laboratories is a multi-program laboratory managed and operated by Sandia Corporation, a wholly owned subsidiary of Lockheed Martin Corporation, for the US Department of Energy's National Nuclear Security Administration under contract DE-AC04-94AL85000. The first author acknowledges the supports by the National Magnetic Confinement Fusion Science Program of China under contract No 2013GB107004, the National Natural Science Foundation of China under Contract No 11375010, 11675218 and the Sino-German Centre for Research Promotion under Contract No GZ769. DIII-D data shown in this paper can be obtained in digital format by following the links at https://fusion.gat.com/global/D3D_DMP.

References

[1] R.A. Pitts, et al., J. Nucl. Mater. 438 (2013) S48.
[2] S. Brezinsek, et al., J. Nucl. Mater. 463 (2015) 11.
[3] G.J. van Rooij, et al., J. Nucl. Mater. 438 (2013) S42.
[4] K. Krieger, et al., J. Nucl. Mater. 266-269 (2013) 207.
[5] R. Dux, et al., J. Nucl. Mater. 390-391 (2009) 858.
[6] C.P.C Wong, et al., J. Nucl. Mater. 258-263 (1998) 433.
[7] W.R. Wampler, et al., J. Nucl. Mater. 438 (2013) S822.
[8] P.C. Stangeby, et al., J. Nucl. Mater. 438 (2013) S309.
[9] A. Kirschner, et al., Nucl. Fusion 40 (2000) 989.
[10] R. Ding, et al., Nucl. Fusion 56 (2016) 016021.
[11] P.C. Stangeby, et al., J. Nucl. Mater. 313-316 (2003) 883.
[12] D.L. Rudakov, et al., Phys. Scr. T159 (2014) 014030.
[13] J.N. Brooks, et al., Fusion Eng. Des. 94 (2015) 67.
[14] R. Chodura, et al., Phys. Fluids 25 (1982) 1628.
[15] J.N. Brooks, Phys. Fluids B 2 (1990) 1858.
[16] P.C. Stangeby, Nucl. Fusion 52 (2012) 083012.
[17] D. Tskhakaya, et al., J. Nucl. Mater. 415 (2011) S860.
[18] D.L. Rudakov, et al., J. Nucl. Mater. 463 (2015) 605.
[19] R. Ding, et al., Plasma Phys. Control. Fusion 51 (2009) 055019.
[20] R. Janev and D. Reiter, (2002) Report Jül-3966, Forschungszentrum Jülich.
[21] A. Kirschner, et al., J. Nucl. Mater. 415 (2011) S23.